ADVANCED TOOLS AND INVERSION METHODS FOR AEM EXPLORATION

Sengpiel, K.-P.[1], and Siemon, B.[1]

1. Federal Institute for Geosciences and Natural Resources (BGR) Hannover, Germany

INTRODUCTION

The applicability of the airborne electromagnetic (AEM) induction method for exploration is a function of the tools available for a determination of the detailed ground resistivity distribution. This includes 3-D outlining of conducting bodies and zones, determination of the thickness and type of sediment above bedrock, tracing of palaeochannels with more or less conductive fill relative to the surroundings, and identification of the fault system and structure of the bedrock. A detailed investigation of the resistivity pattern requires a high-resolution measuring device. Maximum resolution is achieved for “coincident” transmitter and receiver coils (Duckworth *et al.*, 1993), but in practice it is sufficient that the coil spacing s is smaller than the flight altitude h above ground. Mundry (1984) has shown that the well-known integral describing the secondary magnetic field Z measured with a horizontal coplanar coil system above a layered half-space

$$Z = s^3 \int_0^\infty R_0(f, \lambda, \rho_i, d_i)\lambda^2 e^{-2\lambda h} J_0(\lambda s) d\lambda \qquad [1]$$

can be simplified if $s \le 0.3$ h. In the “Mundry integral“ the Bessel function J_0 is replaced by 1 and the coil spacing s has disappeared under the integral. Physically this is equivalent to the “superposed dipole condition“ as postulated by Fraser (1978).

The Mundry integral—without the Bessel function—has a number of favorable features:

a. For a uniform half-space, the integral depends only on the ratio $\delta = h/p$, where p is the half-space skin depth

$$p = \sqrt{2\rho/\omega\mu_0} \qquad [2]$$

This leads to a straightforward inversion of measured data into the true (or apparent) half-space parameters, resistivity ρ (or ρ_a) and distance h (or h_a).

b. The Mundry integral can be used to yield a transfer function C, which provides a depth reference (centroid depth, z^*) to the apparent resistivity ρ_a, calculated from the response of a layered half-space (Sengpiel, 1988). The centroid depth was defined as $z^* = h_a - h + h_a ReC$, using the real part of C, while the imaginary part $ImC \cong -p_a/2$ was not used. Siemon (1996) has shown that it is preferable to use the latter to define $z_p^* = h_a - h + p_a/2$. In Figure 1, a comparison of the sounding curves $\rho_a(z^*)$ and $\rho_a(z_p^*)$ is presented. Only the latter shows the lower conducting layer at the correct depth for this model.

c. The integral can be regarded as a Laplace integral and thus be evaluated numerically very fast (Fluche, 1990). This is of importance for the iterative inversion of measured data into model parameters (see further below).

Applying the above features (a) and (b) to a set of multi-frequency EM data yields a number of corresponding ρ_a, h_a and z^* values, which determine a sounding curve $\rho_a(z_p^*)$ for each measurement site. A color-coded representation of all $\rho_a(z_p^*)$ curves along a flight line provides a resistivity/depth section (“Sengpiel section,” Sengpiel, 1990). Since apparent resistivity values are used in these sections, only a smoothed image of the true resistivity pattern is obtained; the more conductive zones of the ground are over-emphasized relative to the resistive parts.

NEW TYPES OF MULTI-FREQUENCY SOUNDING CURVES

A number of “dynamic” sounding curves, which are more sensitive to vertical resisitivity contrasts, were recently presented by Siemon (1996). The basic ideas were adopted from magnetotellurics and modified for dipole induction. In Figure 1, a dynamic sounding curve $\rho_{NB}(z_p^*)$ is shown which is derived from the standard $\rho_a(z_p^*)$ sounding curve by differentiation $d\rho_a(f)/df$, where f is the frequency. The corresponding centroid depth is $z_s^* = \sqrt{2}z_\rho^*$. Huang and Fraser (1996) presented a similar formulation, but they differentiated the conductance curve with respect to an effective depth z_{eff}, yielding a $\rho_\Delta(z_\Delta)$ sounding curve (Figure 1). While their differentiation is based on discrete ra and z_{eff} values of two neighboring frequencies, the differentiation in our case is conducted after a spline interpolation of the $\rho_a(f)$ curve, which leads to stable results.

Another sensitive sounding curve $\rho_a^\varepsilon(z_p^*)$ is shown in Figure 1. The apparent resisitivity ρ_a^ε is derived simply from the ratio of the quadrature and inphase components of the AEM data and the true flight alti-

In “Proceedings of Exploration 97: Fourth Decennial International Conference on Mineral Exploration” *edited by* A.G. Gubins, 1997, p. 553–556

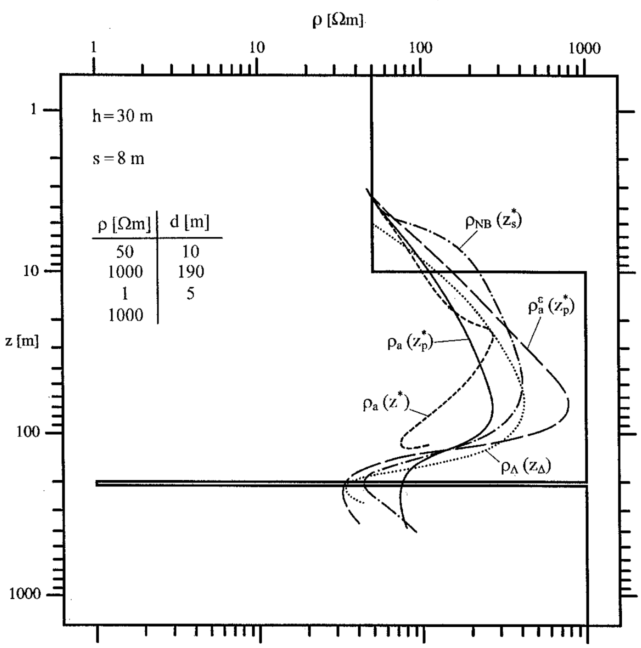

Figure 1: *Sounding curves for a layered half-space model and for frequencies between 50 Hz and 300 000 Hz showing the apparent resistivities* ρ_a *versus the centroid depths* z^* *and* z^*_p*, as well as three "dynamic" sounding curves* $\rho^c_a(z^*_p)$ *and* $\rho_{NB}(z^*_s)$ *, and for comparison* $\rho_\Delta(z_\Delta)$ *after Huang and Fraser (1996). The dynamic sounding curves show a better approximation to the model resistivities than the* ρ_a *sounding curves.*

tude *h* above the ground. The "dynamic" sounding curves are more or less sensitive to inaccurate altitude measurements caused by the vegetation.

IMPROVING MULTI-LAYER INVERSION

A significant improvement of EM multi-frequency sounding was achieved by the development of a Marquardt-type data inversion for the layered half-space model. We use sounding curves to establish a starting model for the iteration process. Another requirement for good inversion results is adequate data quality. This includes a sufficient number of frequencies, a broad frequency range, precisely calibrated data, low drift, and high signal-to-noise ratio. BGR is cooperating with Geoterrex-Dighem in the development of a five-frequency EM bird with five coplanar coil systems for frequencies in the range of 375 Hz to 195 000 Hz. Internal calibration coils provide absolute calibration and phase adjustment during flight without interference from the ground. Details and field data records will be shown in the poster session.

The performance of this five-frequency sensor was examined theoretically using a large number of model calculations (forward calculation and inversion of synthetic data). As will be shown, the 5F data provide a better vertical resolution of resistivity and a larger depth of investigation than 3F data with the same lowest frequency (375 Hz).

INVERSION OF THREE-FREQUENCY FIELD DATA

Figure 2 gives an example of a BGR standard resistivity section with the results of our inversion procedure for a three-layer case. The data (upper part of Figure 2) were produced in the vicinity of Hannover with the BGR 3F-Dighem bird. The dotted line is the trace of the bird altitude above the ground or the vegetation (forest). The layer thicknesses and color-coded resistivities are plotted downward from the tree canopy, which is obtained from measurements with a radar and a barometric altimeter. The top, resistive "layer" corresponds to the vegetation. The second layer (20–60 Ωm, till 6–20 Ωm) and third layer (4–15 Ωm) portray the geology as indicated. Incisions into the clay substratum were caused by glacial meltwater. The glacial channel system can be mapped in great detail using the elevation of the upper boundary of the third layer above sea level.

INVERSION OF DATA FROM 3-D BODIES

The traditional application of AEM is the location of (conducting) 3-D targets. We present a method to determine the depth and the dip of a conductor by an automatic inversion of field data using the centroid depth concept. Figure 3 shows an example as follows:

a. Upper part: The anomalous secondary field data calculated for a horizontal coplanar coil system 30 m above ground for a model of a 40 m thick dike at a depth of 60 m. The dike is 500 m long and its vertical extent is 200 m. The Z_n values on the right give the normal secondary field values for a 100 Ωm half-space. The model calculations were conducted using an algorithm of Xiong (1993), which was kindly made available to B. Siemon.

b. Lower part: A standard resistivity section of ρ_a and z^*_p and the color code is shown. The dotted horizontal lines represent the centroid depths z^*_p for the five frequencies (given above) of the new BGR bird.

For this model, the anomalous field reaches 10 ppm (inphase) for f = 1792 Hz and about 6 ppm for f = 375 Hz. The true depth of 60 m is accurately reproduced by the strong resistivity gradient at this depth. The conducting body causes a broad halo of lower apparent resistivities around it. The limited horizontal extent of 40 m in flight direction is indicated by the field strength minima above the center of the body. Nevertheless, we can conclude that a relatively thin body can be clearly located using a vertical dipole system. Another conclusion is that parameters like the apparent resistivity and the centroid depth, both derived for a half-space model, can readily be used to locate a body of limited extent at the correct depth. The anomaly is likely to be due to current gathering in the body rather than by anomalous induction. Similarly, the minimum ρ_a values in the center of the anomaly are much closer to the bedrock resistivity than to the presumed body resistivity of 0.1 Ωm.

More examples of such model calculations will be shown. This technique of inversion has already been successfully applied to field data from deep sulphide bodies during a AEM survey in Tanzania (Sengpiel, 1991). Poster examples will be shown.

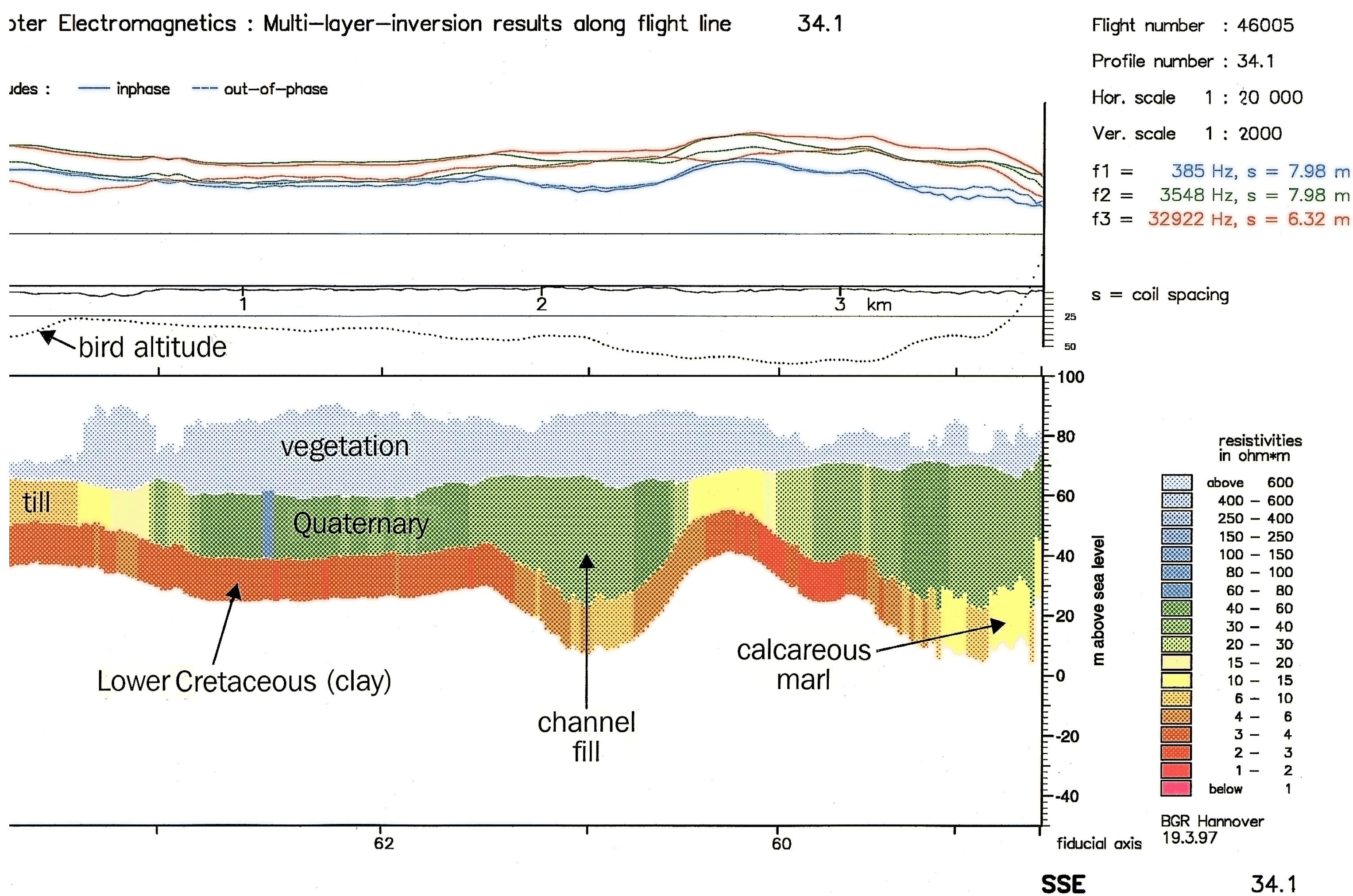

Figure 2: *Resistivity section and associated curves along a flight line near Hannover. From top to bottom: Measured three-frequency data, total error of inversion, EM bird altitude (dotted curve), and color-coded resistivity section, in which the results of a Marquardt-type data inversion including the forest "layer" are shown. The BGR survey outlined the glacial channel system incised into the clay substratum.*

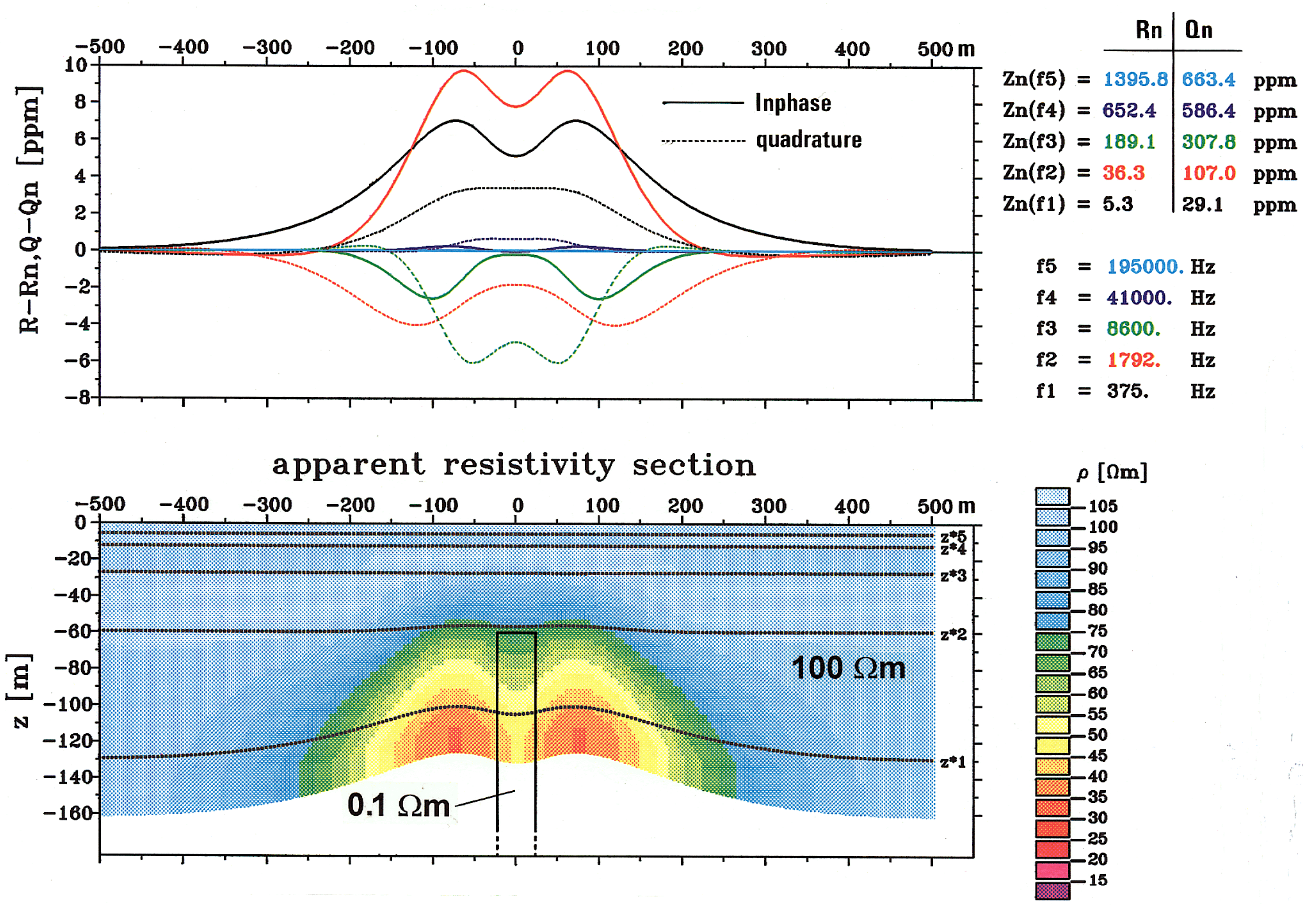

Figure 3: *Anomalous secondary field values (top) calculated for the 3-D model shown below. The color-coded resistivity section (below) was obtained using the* $\rho_a(z^*_p)$ *sounding curve concept as explained in the text. The (symmetric) halo of lower resistivities around the conductor indicates its depth and (vertical) dip.*

REFERENCES

Duckworth, K., Krebes, E. S., Juigalli, J., Rogozinski, A. and Calvert, H. T., 1993. A coincident-coil frequency-domain electromagnetic prospecting system. Can. J. Expl. Geophys., **29**, 411-418.

Fluche, B., 1990. Verbesserte Verfahren zur Lösung des direkten und des inversen Problems in der Hubschrauber-Elektromagnetik. In: Haak, V. and Homilius, J. (eds): Protokoll Kolloquium Elektromagnetische Tiefenforschung, Hornburg, 249-266.

Fraser, D. C., 1978. Resistivity mapping with an airborne multicoil electromagnetic system. Geophysics, **43**, 144-172.

Huang, H. and Fraser, D. C., 1996. The differential parameter method for multifrequency airborne resistivity mapping. Geophysics, **61**, 100-109.

Mundry, E., 1984. On the interpretation of airborne electromagnetic data for the two-layer case. Geophys. Prosp., **32**, 336-346.

Sengpiel, K.-P., 1988. Approximate inversion of airborne EM data from a multilayered ground. Geophys. Prosp., **36**, 446-459.

Sengpiel, K.-P., 1990. Theoretical and practical aspects of ground-water exploration using airborne electromagnetic techniques. In: Fitterman, D. V. (ed.), Proceedings of the USGS Workshop on Developments and Applications od Modern Airborne Electromagnetic Surveys, 1987, Golden, Colo., USGS Bulletin 1925, 149-154

Sengpiel, K.-P., 1991. BGR helicopter survey 1988 in Tanzania—Selection of conductivity anomalies as targets for prospecting sulphide mineralization. BGR-Archives No.: 107 958, (unpublished report), Hannover.

Siemon, B., 1996. Neue Verfahren zur Berechnung von scheinbaren spezifischen Widerständen und Schwerpunktstiefen in der Hubschrauberelektromagnetik. In: Bahr, K. and Junge, A.(eds): Protokoll Kolloquium Elektromagnetische Tiefenforschung, Burg Ludwigstein.

Xiong, Z., 1993. Electromagnetic modeling of three-dimensional structures in stratified anisotropic earths using the integral equation method. In: Schmucker, U. (ed.) Entwicklung und Erprobung von Algorithmen zu dreidimensionalen Modellrechnungen in der Erdmagnetischen Tiefensondierung, Report for project Schm 101/15, Univ. Göttingen.